Hindawi Publishing Corporation
Journal of Nanomaterials
Volume 2015, Article ID 513814, 10 pages
http://dx.doi.org/10.1155/2015/513814

Research Article

Experimental Study on the Deactivating Effect of KNO_3, KCl, and K_2SO_4 on Nanosized Ceria/Titania SCR Catalyst

Xiongbo Chen,[1,2] Ping Fang,[1,2] Wenhao Zeng,[1,2] Kunyuan Liu,[3] Zhixiong Tang,[1,2] and Chaoping Cen[1,2]

[1]*South China Institute of Environmental Sciences, The Ministry of Environmental Protection of PRC, No. 7 West Street, Yuancun, Guangzhou 510655, China*
[2]*The Key Laboratory of Water and Air Pollution Control of Guangdong Province, No. 7 West Street, Yuancun, Guangzhou 510655, China*
[3]*School of Chemical Engineering and Technology, Tianjin University, Tianjin Weijin Road, No. 92, Nankai District 300072, China*

Correspondence should be addressed to Chaoping Cen; cenchaoping@scies.org

Received 29 June 2015; Revised 24 August 2015; Accepted 25 August 2015

Academic Editor: Bao Yu Xia

Copyright © 2015 Xiongbo Chen et al. This is an open access article distributed under the Creative Commons Attribution License, which permits unrestricted use, distribution, and reproduction in any medium, provided the original work is properly cited.

Nanosized Ce/TiO_2 is effective in selective catalytic reduction of NO with NH_3. The NO conversion of Ce/TiO_2 is 93% at 370°C. However, addition of potassium using KNO_3, KCl, or K_2SO_4 as precursors effectively deactivates Ce/TiO_2. NO conversion at 370°C is reduced to 45%, 24%, and 16% after addition of KNO_3, KCl, and K_2SO_4, respectively, with a controlled K/Ce molar ration at 0.25. The deactivation may be attributed to the changes in the structural and chemical state of ceria and the degradation of surface acidity. The transformation of amorphous ceria into ceria crystals after potassium addition, together with the decrease of surface defects, is also determined. Oxygen diffusion in the process of ceria reduction is slow, and the redox cycle is slowed down. Moreover, the surface acid sites are markedly destroyed, leading to the reduced capacity of ammonia adsorption. These results may provide useful information for the application and life management of CeO_2/TiO_2 in potassium-rich environments such as biofuel-fired boilers.

1. Introduction

Selective catalytic reduction (SCR) of NO with ammonia is the most efficient and reliable technology to remove NO_x from stationary sources. $V_2O_5(WO_3)/TiO_2$ or $V_2O_5(MoO_3)/TiO_2$ catalysts are widely used in the SCR process. These vanadium-based catalysts are highly efficient. However, V_2O_5 is an ecotoxic material that is harmful to the environment [1]. To replace vanadium-based catalysts, environment-friendly, nonvanadium catalysts such as Ce/TiO_2, $Mn_2Nb_1O_x$, MnO_x-CeO_y, Fe-ZSM-5, Cu-ZSM-5, and $FeTiO_x$ have been developed in the past years [2–8].

Recently, Ce/TiO_2 catalyst has gained recognition because of its excellent activity and selectivity. Xu et al. reported that Ce/TiO_2 catalyst is highly efficient at 275–400°C, and the undesired by-product, N_2O, could be hardly detected [3]. Gao et al. compared three preparation methods, namely, single step sol-gel method, impregnation method, and coprecipitation method, and found that the Ce/TiO_2 catalysts prepared using the single step sol-gel method had the best SCR activity and SO_2 resistance. Liu et al. demonstrated the feasibility of a supercritical water synthesis route in the syntheses of Ce/TiO_2 catalysts by a strong metal-support interaction [9]. Chen et al. found that tungsten modification could further improve the activity of Ce/TiO_2 [10], and Liu et al. used MoO_3 modification to enhance this activity. Chen et al. investigated a series of ceria catalysts supported on titanates with various morphologies and structures, including nanoparticle, nanotube, fragment, nanowire, and nanorod; the investigation revealed a good SCR performance of the former three catalysts. Moreover, Ce/TiO_2-based catalysts have been commercially produced in rare earth-rich regions such as Shandong, China, and utilized in deNOx facilities in power plants.

While nonvanadium SCR catalysts were developed, the deactivation of SCR catalysts by alkali metals and alkaline

earth metals has gained popularity. This problem has been proven to be more serious in biofuel boilers because alkali metal content is higher in biofuels than in coal. For vanadium-based catalysts, many studies in literature noted the decrease of surface acidity by potassium, sodium, and calcium compounds, and a few works found the interaction between poison and vanadium sites [11, 12]. Moreover, Strege et al. proposed that the blocking of surface pores is an important reason for this observation. As for Fe-ZSM-5, Kern et al. attributed alkali deactivation to the decreased capability of ammonia adsorption [13]. Similar results of Fe- and Cu-based catalysts supported on TiO_2 or ZrO_2 were reported by Kustov et al. [14]. With respect to CeO_2/TiO_2 catalysts, Wang et al. investigated the significant deactivation by sodium and calcium salts and proposed a deactivation mechanism based on the change of the ceria state [15]. Some other catalysts, such as Cu-SAPO-34 and MnO_x/TiO_2, also encountered a similar deactivation [16, 17]. Considering the extensive knowledge of alkali deactivation of various catalysts, the application of SCR technology to the purification of biofuel flue gas is questionable.

In this paper, we investigated the poisoning effect of various potassium compounds on nanosized Ce/TiO_2 catalysts in the SCR application. KCl and K_2SO_4 were selected as the precursors of potassium because the potassium content is very high in the flue gas of boilers firing biofuels, and Cl and S elements always coexist [18, 19]. KNO_3 was selected as the precursors of potassium oxide. Fresh and K-poisoned Ce/TiO_2 catalysts were subjected to a range of characterizations (e.g., XRD, XPS, NH_3-TPD, and H_2-TPR), and the deactivation mechanism was discussed.

2. Experimental

2.1. Preparation of Ce/TiO_2 Catalyst. Commercially produced P25 TiO_2 (Degussa, Germany) was used as the catalyst support. Cerous nitrate (AR, $Ce(NO_3)_3{\cdot}6H_2O$) was used as the precursor of ceria. Ceria was loaded on P25 TiO_2 using the wet-impregnation method with a controlled Ce/Ti molar ratio of 1 : 19. In summary, P25 was impregnated in a cerous nitrate solution, and the mixture was stirred for 4 h, dried at 80°C for 12 h, and calcined at 450°C for 3 h.

2.2. Addition of Potassium Compounds. As described in previous reports, adding potassium in various concentrations was always conducted by the wet-impregnation method to simulate the poisoning mechanism of potassium in real flue gas at laboratory [16, 20]. In this paper, KNO_3, KCl, and K_2SO_4 were dissolved in distilled water and impregnated with Ce/TiO_2 catalysts. The mixture was stirred vigorously for 4 h, dried at 80°C for 12 h, and calcined at 450°C for 3 h. The K/Ce molar ratio was controlled at 0.25, 0.5, 1, and 2. The prepared catalysts were denoted as Ce/TiO_2-*x*-*y*, where *x* are the precursors (KNO_3, KCl, and K_2SO_4) and *y* is the K/Ce molar ratios (0.25, 0.5, 1, and 2).

2.3. SCR Activity Evaluation. SCR activities on fresh and K-poisoned Ce/TiO_2 catalysts were tested in a fixed-bed reactor. The typical reactant gas composition was as follows: 750 ppm NO, 750 ppm NH_3, 1.5% H_2O, 3.5% O_2, and balanced N_2. The catalyst dosage was 0.5 g. The gas hourly space velocity (GHSV) was approximately 100,000 h^{-1}. NO, NO_2, and O_2 concentrations were monitored by a flue gas analyzer (KM9106, Quintox Kane International Limited). N_2O was detected by a FT-IR gas analyzer (Madur Photon Portable IR Gas Analysers, Madur Ltd., Austria).

2.4. Characterization Methods. XRD analysis was performed using X-ray diffraction with Cu Kα radiation (model D/max RA, Rigaku Co., Japan). The data were collected for scattering angles (2θ) ranging between 5° and 80° with a step size of 0.02°. X-ray photoelectron spectroscopy with Al Kα X-ray ($h\nu$ = 1486.6 eV) radiation operated at 150 W (XPS: Thermo ESCALAB 250, USA) was used to investigate the surface properties and probe the electronic state of the elements. The microstructures were observed using a scanning electron micrograph (SEM) in a Phillips XL-30-ESEM system with a voltage of 15 kV. Nitrogen adsorption-desorption isotherms were obtained using a nitrogen adsorption apparatus (ASAP 2020, USA). All the samples were degassed at 200°C prior to measuring. The Brunauer-Emmett-Teller (BET) specific surface area (SBET) was determined by a multipoint BET method using the adsorption data in the relative pressure ($P/P0$) range from 0.05 to 0.30. Temperature programmed desorption with ammonia (NH_3-TPD) and temperature programmed reduction with hydrogen (H_2-TPR) experiments were carried out using a TP-5080 instrument (Tianjin Xianquan Industry and Trade Development Co. Ltd., China). Prior to the NH_3-TPD experiments, 100 mg samples were pretreated in pure N_2 at 350°C for 1 h and then saturated with anhydrous NH_3 (4% in N_2) at room temperature. Desorption was carried out by heating the samples in N_2 (30 mL/min) from 70°C to 800°C with a heating rate of 10°C/min. Before raising the temperature, a preheat treatment at 70°C for 1 h was conducted. For the TPR experiments, 50 mg samples were pretreated in pure N_2 at 350°C for 1 h and cooled to 70°C. The H_2-TPR runs were carried out with a linear heating rate of 10°C/min from 70°C to 800°C in H_2 (4% in N_2).

3. Results and Discussion

3.1. SCR Performance. Figures 1–3 show NO conversions as a function of the reaction temperature over catalysts with different loading amounts of KNO_3, KCl, and K_2SO_4, respectively. The fresh Ce/TiO_2 catalyst shows good catalytic activity in the temperature range of 285°C to 460°C. The NO conversion reaches up to 93% at 370°C. However, the NO conversion rapidly decreases after adding potassium. When the K/Ce molar ration exceeds 0.25, NO conversion becomes negligible in the entire temperature range regardless of the precursors. Relatively, the addition of KCl or K_2SO_4 is more harmful to the SCR activity of Ce/TiO_2 than that of KNO_3. The NO conversion at 370°C in Ce/TiO_2-KNO_3-0.25 is consistent at 45%, but it is kept at 16% and 24% in Ce/TiO_2-K_2SO_4-0.25 and Ce/TiO_2-KCl-0.25, respectively.

To find the internal reasons for the deactivation by potassium salts, Ce/TiO_2, Ce/TiO_2-KNO_3-0.25, Ce/TiO_2-K_2SO_4-0.25, and Ce/TiO_2-KCl-0.25 were subjected to a range

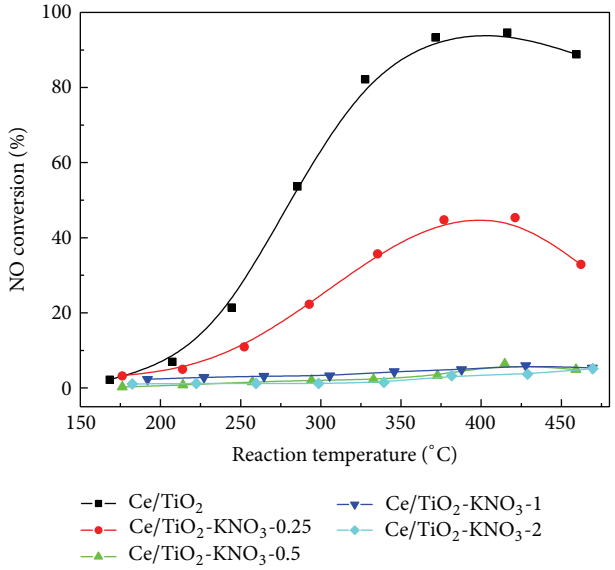

Figure 1: Variation of NO conversion with reaction temperature of catalysts with different KNO_3 loading.

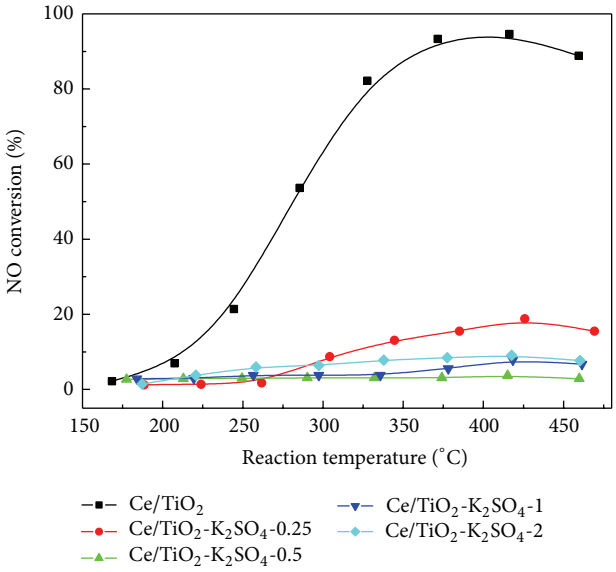

Figure 2: Variation of NO conversion with reaction temperature of catalysts with different K_2SO_4 loading.

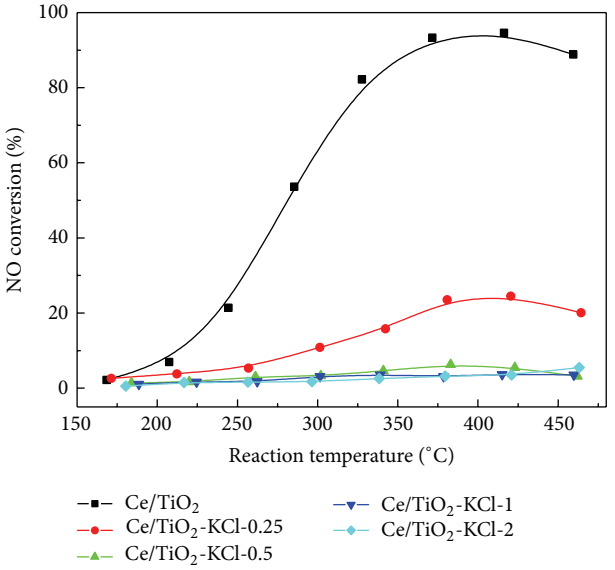

Figure 3: Variation of NO conversion with reaction temperature of catalysts with different KCl loading.

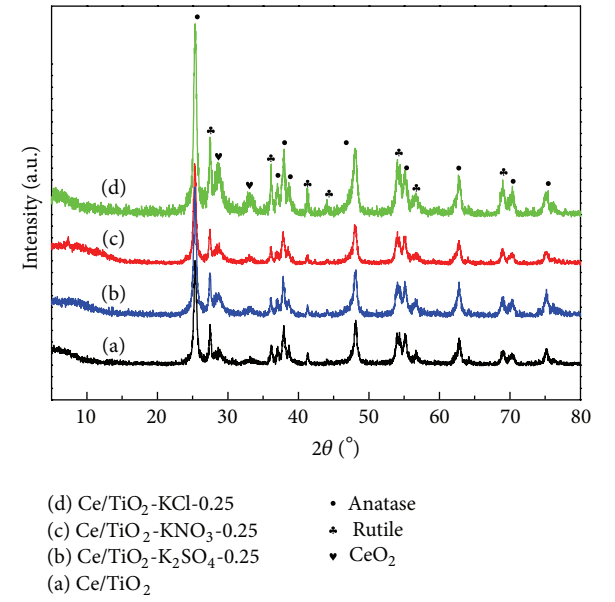

Figure 4: Powder XRD patterns of fresh and K-poisoned Ce/TiO_2 catalysts.

of characterizations including XRD, BET-BJH, XPS, NH_3-TPD, and H_2-TPR.

3.2. Crystal Structure and Morphology. The powder XRD patterns of fresh and K-poisoned Ce/TiO_2 catalysts are shown in Figure 4. Characterization peaks in the anatase phase (PDF-number 21-1272, $2\theta = 25.28^\circ$, 37.80°, 48.05°, 53.89°, 55.06°, and 62.69°) and rutile phase (PDF-number 21-1276, $2\theta = 27.45^\circ$, 36.09°, and 54.32°) appear in all the four catalysts. The characterization peaks of ceria (PDF-number 43-1002, $2\theta = 28.55^\circ$, 33.08°, 47.48°, and 56.33°) are not noticeable in Ce/TiO_2 but become clear after adding potassium. As described in Experimental, the Ce/Ti molar ration was designed at 1 : 19; hence the weight percentage of ceria in the Ce/TiO_2 catalyst is approximately 10% which is above the detection limit of XRD. As such, the changes of ceria peaks suggest that highly dispersing amorphous ceria as very small nanoparticles is the dominant structure of ceria in the fresh Ce/TiO_2 catalyst but transforms into ceria crystals in the K-poisoned catalysts. The particle size of ceria, which is calculated by plane [111] using the Scherrer Equation, grows to 7.6–7.9 nm in the three K-poisoned catalysts. Notably, the intensity of ceria peaks follows the following sequence: Ce/TiO_2-KCl-0.25 > Ce/TiO_2-K_2SO_4-0.25 > Ce/TiO_2-KNO_3-0.25, indicating that

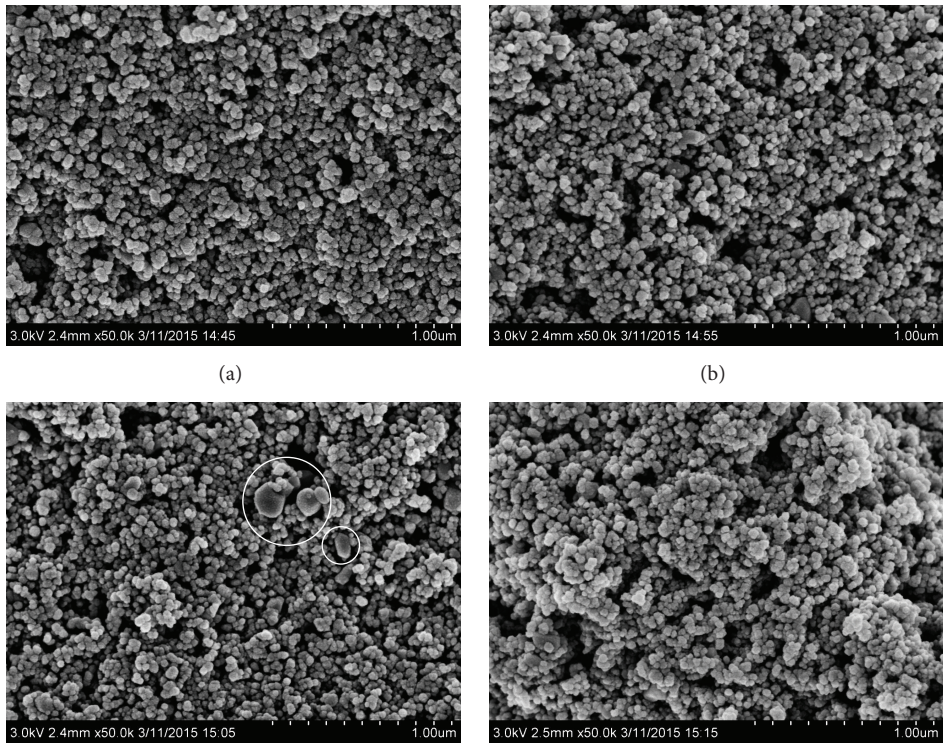

Figure 5: SEM images of Ce/TiO_2 (a), Ce/TiO_2-KNO_3-0.25 (b), Ce/TiO_2-KCl-0.25 (c), and Ce/TiO_2-K_2SO_4-0.25 (d).

the crystallinity of ceria in the three catalysts may also follow the same order.

Microstructures of the fresh and K-poisoned Ce/TiO_2 catalysts observed by SEM are shown in Figure 5. The surface of fresh Ce/TiO_2 catalyst is smooth when viewed through SEM (Figure 5(a)). The aggregation of particles cannot be observed. However, different degrees of aggregation can be observed in K-poisoned catalysts. Interstices between particles are enlarged. Variant large particles appear in the SEM image of Ce/TiO_2-KCl-0.25. Considering the highest intensities of ceria and titania XRD peaks in Ce/TiO_2-KCl-0.25, the destructive effect of KCl may have possibly occurred on ceria and titania particles. High-grade aggregation was observed in Ce/TiO_2-K_2SO_4-0.25, and the surface becomes bumpy like heaped-up hills. Microstructures indicate that the dispersion of constituent particles worsened in K-poisoned catalysts, especially in KCl- and K_2SO_4-poisoned catalysts.

Morphology, structure, and particle size of the fresh and K-poisoned Ce/TiO_2 catalysts further observed by TEM are shown in Figure 6. Aggregation can also be observed in K-poisoned catalysts like SEM images. Some ceria particles are circled in red. A small number of ceria particles can be observed in the fresh Ce/TiO_2 catalyst. However, in K-poisoned catalysts, the number of ceria particles increases significantly, and overgrowth of ceria particles occurs in Ce/TiO_2-KCl-0.25 and Ce/TiO_2-K_2SO_4-0.25. The obvious difference in the number of ceria particles between fresh and K-poisoned Ce/TiO_2 catalysts further confirms the increasing crystallization of ceria after K-loading. The TEM results are in good agreement with the XRD and SEM discussions. Therefore, the transformation of highly dispersing amorphous ceria to worse dispersing ceria crystals is certain.

3.3. Physical Characterizations. Table 1 shows the physical characterizations including BET surface area, pore volume, and average pore diameter. Compared with the BET surface area, pore volume, and average pore diameter of Ce/TiO_2, those of Ce/TiO_2-K_2SO_4-0.25 reduced slightly, indicating that part of the K_2SO_4 may deposit on the catalyst surface and cover a few pores. For Ce/TiO_2-KCl-0.25 and Ce/TiO_2-KNO_3-0.25, the BET surface areas are reduced further, pore volumes are not reduced, and average pore diameters slightly increased, suggesting that a few pores agglomerate and enlarge along with the growth of ceria crystals. All the changes mentioned in the physical characterizations accorded well with the microstructures showed by SEM. Notably, the changes in physical characterizations were slight. Hence adding potassium has very limited effect on the physical characterizations of Ce/TiO_2. The changes in physical characterizations are not the primary reason for deactivation.

3.4. Surface Species. The surface atomic concentrations of Ce, Ti, O, K, Cl, and S acquired with XPS are shown in Table 2. As revealed by XRD, highly dispersed amorphous ceria transforms into ceria crystals after adding potassium. Generally, amorphous ceria interacts closely with the TiO_2 support; however ceria crystals are more independent and tend to agglomerate. Hence the surface atomic concentrations

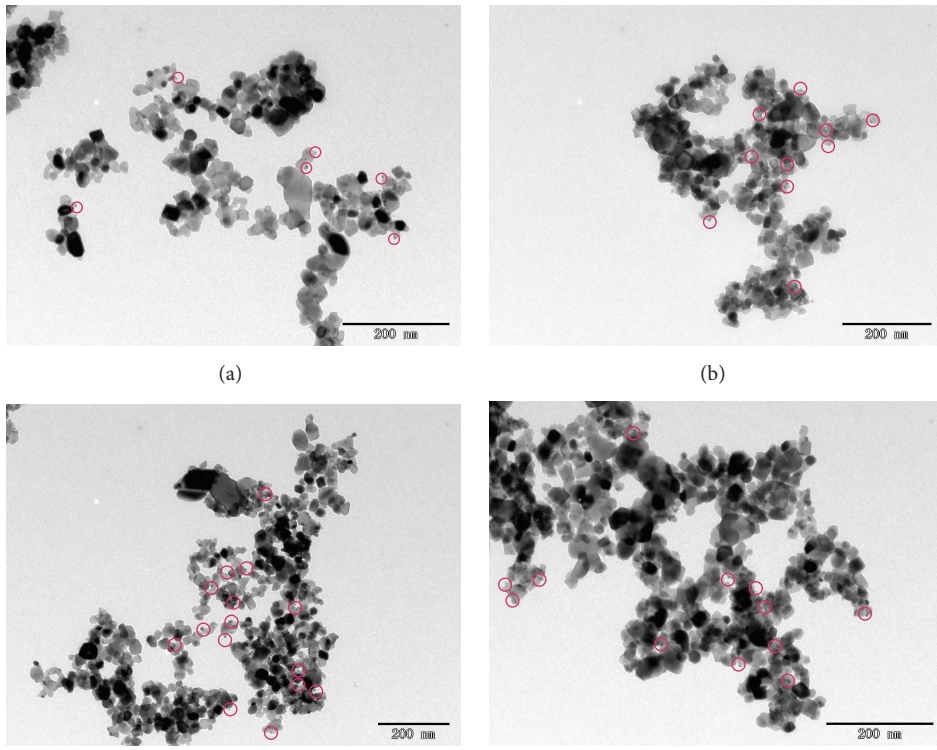

(a) (b)

(c) (d)

Figure 6: TEM images of Ce/TiO_2 (a), Ce/TiO_2-KNO_3-0.25 (b), Ce/TiO_2-KCl-0.25 (c), and Ce/TiO_2-K_2SO_4-0.25 (d).

Table 1: BET surface area, pore volume, and average pore diameter.

Sample	BET surface area (m^2/g)	Pore volume (cm^3/g)	Average pore diameter (nm)
Ce/TiO_2	45.9	0.40	28.55
Ce/TiO_2-KNO_3-0.25	42.8	0.40	30.57
Ce/TiO_2-K_2SO_4-0.25	45.0	0.39	28.03
Ce/TiO_2-KCl-0.25	41.7	0.41	31.59

Table 2: Surface atomic concentrations of various elements acquired with XPS.

Sample	Ce	Ti	O	K	Cl	S
Ce/TiO_2	1.86	31.60	66.54	—	—	—
Ce/TiO_2-KNO_3-0.25	2.01	32.22	65.00	0.76	—	—
Ce/TiO_2-KCl-0.25	2.13	31.49	64.92	0.99	0.47	—
Ce/TiO_2-K_2SO_4-0.25	2.29	30.41	64.43	1.76	—	1.11

of Ce increase after adding potassium. The atomic concentrations of K, Cl, N, and S gave some evidence of the final form of potassium poisons. N atoms are hardly detected in Ce/TiO_2-KNO_3-0.25, indicating that KNO_3 has decomposed into K_2O. The atomic concentration of the K surface is higher in Ce/TiO_2-K_2SO_4-0.25 than in Ce/TiO_2-KCl-0.25 and Ce/TiO_2-KNO_3-0.25 which may be attributed to the deposition of K_2SO_4 on the surface of Ce/TiO_2-K_2SO_4-0.25. The atomic concentration of K in Ce/TiO_2-KCl-0.25 is more than twice that of Cl, suggesting that Cl can enter into the catalyst bulk.

The XPS spectra of Ce 3d are shown in Figure 7, where peaks labeled as u, u2, u3, v, v2, and v3 represent the $3d^{10}4f^0$ state of Ce^{4+} species, and those labeled as u1 and v1 represent the $3d^{10}4f^1$ initial electronic state corresponding to Ce^{3+} species [21, 22]. Generally, Ce^{4+} is dominant in fine ceria crystals, and Ce^{3+} accompanied with ceria defects is abundant in small ceria particles such as amorphous ceria. The intensity of Ce^{4+} is always measured in terms of peak area proportion of u3 in the whole spectrum. As shown in Table 3, the peak area proportion of u3 increases after adding potassium. This finding reveals that the concentration of ceria defects is reduced and the XRD results have confirmed the transformation of amorphous ceria into ceria crystals.

The fitted XPS spectra of O 1s are shown in Figure 8. The O 1s peaks mainly contain two different species: crystal lattice oxygen (O_α) and chemisorbed oxygen (O_β) [21, 23, 24]. The O_α peak is located at 529.92 eV in the spectrum of Ce/TiO_2

Table 3: Peak areas of the fitted O 1s and Ce 3d XPS spectra.

Sample	Peak area of O 1s			Peak area of Ce 3d		
	O_α	O_β	Proportion of O_β	u3	Whole spectrum	Proportion of u3
Ce/TiO_2	130585	19085	12.75%	5283	77795	6.79
Ce/TiO_2-KNO_3-0.25	135300	17500	11.45%	6186	73603	8.40
Ce/TiO_2-KCl-0.25	128985	14285	9.97%	6783	80462	8.43
Ce/TiO_2-K_2SO_4-0.25	146085	21501	12.83%	9547	89451	10.67

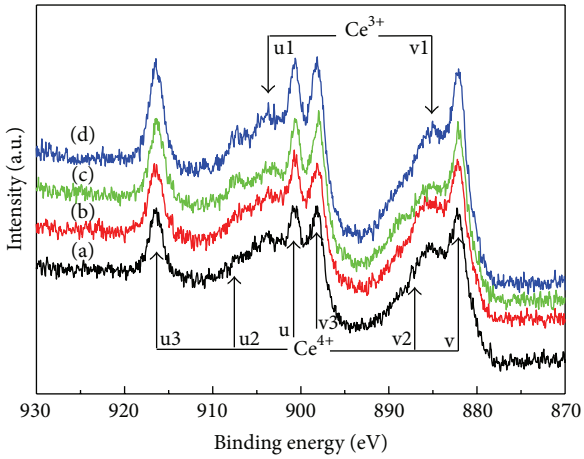

(a) Ce/TiO_2 (c) Ce/TiO_2-KCl-0.25
(b) Ce/TiO_2-KNO_3-0.25 (d) Ce/TiO_2-K_2SO_4-0.25

Figure 7: XPS spectra of Ce 3d.

but shifts to a lower binding energy in the spectra of K-poisoned catalysts. This shift can often be observed during the transformation of Ce^{3+} into Ce^{4+} [21, 23, 24]. Chemisorbed oxygen has been proven to be active in oxidation reactions and will take part in the oxidation of Ce^{3+} to Ce^{4+}. The concentration of chemisorbed oxygen is assumed to be positively related with the ceria defects. As a result, the concentration of chemisorbed oxygen should decrease after adding potassium addition (see Table 3). The concentrations of chemisorbed oxygen in Ce/TiO_2-KCl-0.25 and Ce/TiO_2-KNO_3-0.25 are lower than that of Ce/TiO_2, as expected. However, the chemisorbed oxygen concentration in Ce/TiO_2-K_2SO_4-0.25 is slightly higher and may be contributed by the SO_4^{2-} groups. As reported by Gao et al., sulfurization treatment could provide new chemisorbed oxygen in the form of –OH or H_2O groups [25].

3.5. Surface Acidity and Reducibility. According to the widely accepted Eley-Rideal and Langmuir-Hinshelwood mechanism of SCR reaction [26, 27], the adsorption of NH_3 on the catalyst surface s is considered a prerequisite. The NH_3-TPD profiles of the four catalysts are shown in Figure 9, where the decreased NH_3-desorption can be observed in the K-poisoned samples. The total amount of desorbed ammonia is calculated at 209 μmol/g, 141 μmol/g, 119 μmol/g, and 157 μmol/g over Ce/TiO_2, Ce/TiO_2-KNO_3-0.25, Ce/TiO_2-KCl-0.25, and Ce/TiO_2-K_2SO_4-0.25, respectively, showing a noticeable decrease. The desorbed ammonia corresponds to the ammonia adsorbed on the Lewis and Brønsted acid sites. Hence these acid sites were partly destroyed by potassium after addition.

It is widely accepted that the reduction of ceria can be divided into two processes: the initial reduction of surface ceria species at low temperature and the further reduction of bulk ceria at high temperature. Considering the XRD and XPS results, we can deduce that amorphous ceria with abundant defects in Ce/TiO_2 tends to be reduced at low temperatures, whereas ceria crystals in K-poisoned catalysts reduce at high temperatures [28, 29]. As depicted in Figure 10, the reduction of ceria starts at 261°C in Ce/TiO_2, and the reduction maximum appears at 487°C. However, the starting temperature shifts to the right at 444°C, 457°C, and 377°C in the profiles of Ce/TiO_2-KNO_3-0.25, Ce/TiO_2-KCl-0.25, and Ce/TiO_2-K_2SO_4-0.25, respectively. This finding demonstrates that the addition of potassium leads to the passivating of ceria, similar to the transformation of amorphous ceria into ceria crystals. Moreover, there are sharp reduction peaks centering at 718°C and 652°C in the H_2-TPR profiles of Ce/TiO_2-KCl-0.25 and Ce/TiO_2-K_2SO_4-0.25, respectively. Similar peaks are not found in the H_2-TPR profile of Ce/TiO_2-KNO_3-0.25, demonstrating that the crystallinity of ceria in Ce/TiO_2-KCl-0.25 and Ce/TiO_2-K_2SO_4-0.25 is higher.

3.6. Deactivation Mechanism. Based on the analysis above, the changes that take place after adding potassium are summarized in Table 4. We can find two main reasons for the deactivation of Ce/TiO_2 catalyst by potassium: the structural and chemical state changes of ceria and the degradation of surface acidity.

In terms of ceria catalysts, good redox behavior in catalysis reactions involves high-speed Ce^{4+}/Ce^{3+} redox cycles. Previous researches on the redox behavior of ceria have shown that the oxidation of Ce^{3+} to Ce^{4+} is very fast, whereas the reduction of Ce^{4+} to Ce^{3+} is slow in most cases [30]. Oxygen diffusion that depends on the type, size, and concentration of oxygen vacancies is proposed to be the rate-controlling step of ceria reduction [30–32]. Therefore, the nature of oxygen vacancy highly affects the redox behavior of ceria. It is known that once Ce^{3+} appears, oxygen vacancies will be generated to maintain electrostatic balance [32, 33]. Consequently, ceria defects on the catalyst surface are the most active species with fast Ce^{4+}/Ce^{3+} redox cycle. For the Ce/TiO_2 catalyst, ceria mainly exists in a highly dispersed amorphous form with surface having abundant defects; hence

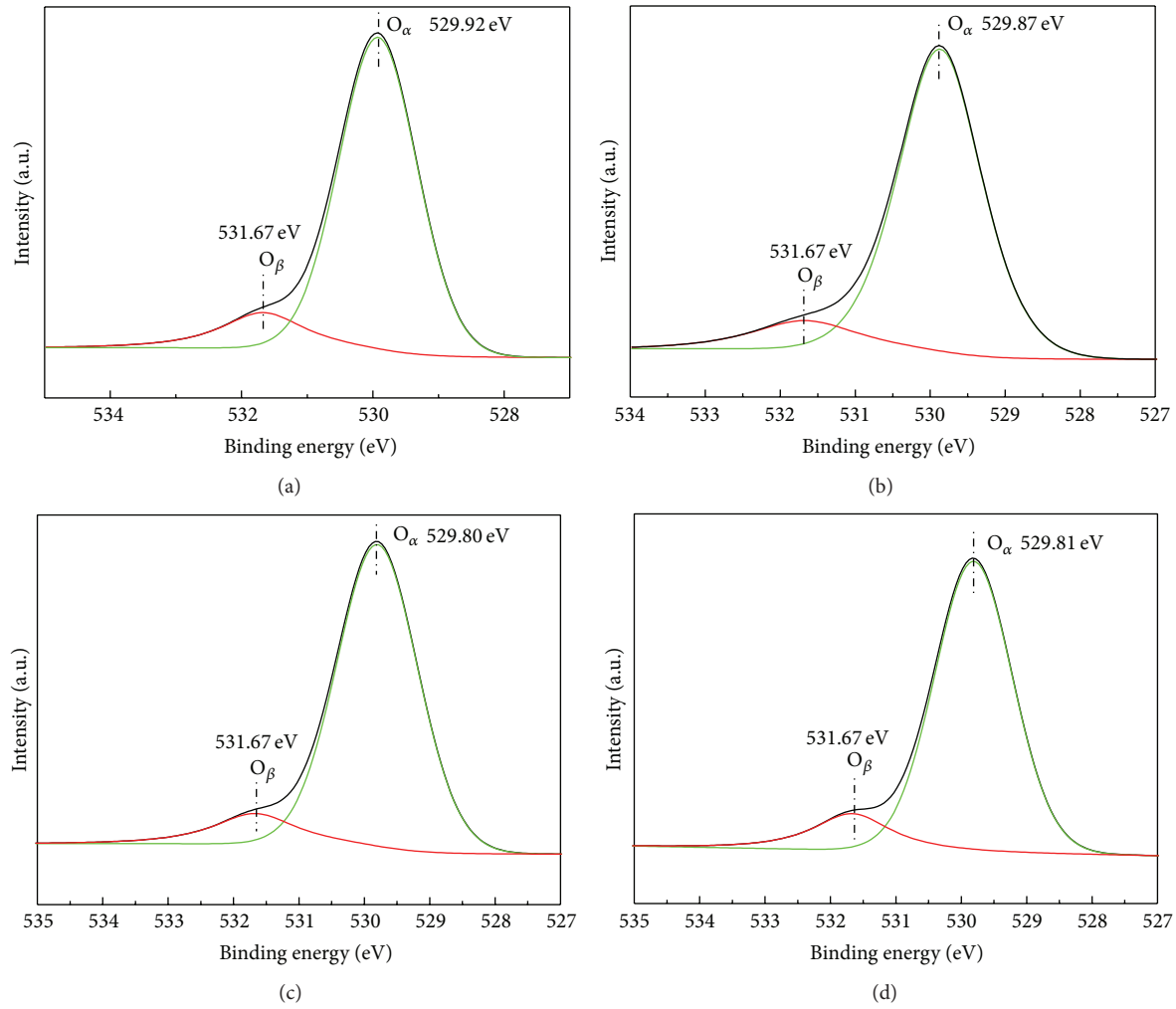

Figure 8: XPS spectra of O 1s: (a) Ce/TiO_2, (b) Ce/TiO_2-KNO_3-0.25, (c) Ce/TiO_2-KCl-0.25, and (d) Ce/TiO_2-K_2SO_4-0.25.

Table 4: Sum of the property changes after potassium addition.

Sample	Crystal structure of ceria	Microstructure	Chemical state of cerium	Ammonia adsorption	Reducibility of ceria	SCR performance
Ce/TiO_2-KNO_3-0.25	Amorphous to crystal	Enlarged interstices	Decrease of Ce^{3+}	Reduced NH_3 adsorption	Passivating of ceria	Deactivation
Ce/TiO_2-KCl-0.25	Highest crystallinity	Variant particles	Decreased of Ce^{3+}	Largest decrease of NH_3 adsorption	Serious passivating of ceria	Serious deactivation
Ce/TiO_2-K_2SO_4-0.25	High crystallinity	High aggregation	Largest decrease of Ce^{3+}	Reduced NH_3 adsorption	Serious passivating of ceria	Serious deactivation

the reduction of ceria can start at very low temperature (261°C), and the Ce/TiO_2 shows good SCR performance. For K-poisoned catalysts, amorphous ceria transforms into ceria crystals, and the size of ceria particles enlarges. As a result, the amount of surface defects, as well as oxygen vacancies, is reduced which hinders the reduction of ceria in the redox cycle. The reduction of ceria only occurred at higher temperatures. The K-doped catalysts showed the worst SCR performance. Notably, a more complete transformation of the structural and chemical state of ceria can be observed after adding KCl and K_2SO_4; hence the deactivation by the addition of KCl and K_2SO_4 is more significant than adding KNO_3.

The degradation of the surface acidity is considered a common reason for all the SCR catalysts that underwent alkali deactivation. It is widely accepted that the acid sites on

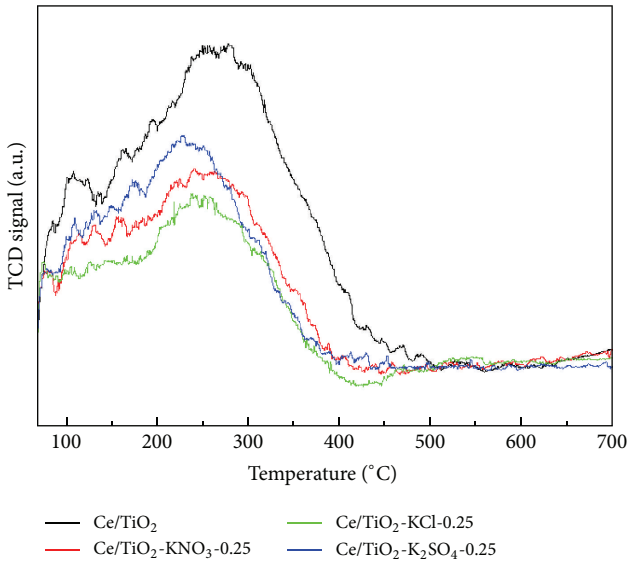

FIGURE 9: NH_3-TPD profiles of Ce/TiO_2, Ce/TiO_2-KNO_3-0.25, Ce/TiO_2-KCl-0.25, and Ce/TiO_2-K_2SO_4-0.25.

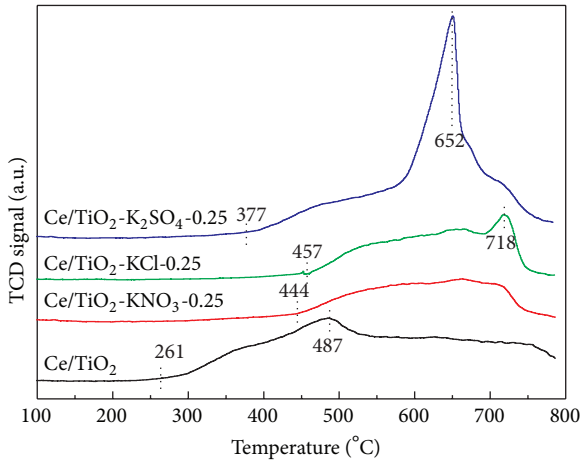

FIGURE 10: H_2-TPR profiles of Ce/TiO_2, Ce/TiO_2-KNO_3-0.25, Ce/TiO_2-KCl-0.25, and Ce/TiO_2-K_2SO_4-0.25.

the catalyst surface can be easily destroyed by alkaline species. Hence the decreasing capacity of ammonia adsorption by potassium has always been observed in V-, Fe-, Cu-, and zeolite-based catalysts [11–14, 16, 17]. For the Ce/TiO_2 catalyst, we have found apparent degradation of the surface acidity regardless of the difference of the potassium precursor.

It is interesting to note that the Cl^- and SO_4^{2-} anions have additional poisoning effects. Lisi et al. have reported that acidic HCl can promote the formation of new acid sites on the vanadium-based catalysts [34], indicating that Cl^- may be beneficial to surface acidity. However, this positive effect of Cl^- is not found on KCl-doped CeO_2/TiO_2 catalyst. In the three catalysts, the largest decrease of NH_3 adsorption is observed in the KCl-doped catalyst. The extra decrease may be associated with Cl^-. From XPS results, we have deduced that Cl^- can enter freely into the catalyst bulk. Cl^- may combine with Ce to form cerium chloride and destroy the Ce-centered Lewis acid sites. High-grade aggregation of the whole catalyst sample is observed in K_2SO_4-doped catalysts. The aggregation that attributed to the deposition of K_2SO_4 on catalyst surface will reduce the exposure of active sites for the SCR reaction.

4. Conclusions

The addition of KNO_3, KCl, and K_2SO_4 could deactivate the Ce/TiO_2 catalyst in a SCR reaction. After adding KNO_3, KCl, or K_2SO_4 with a K/Ce molar ration of 0.25, the NO conversion at 370°C dropped sharply from 93% to 45%, 24%, and 16%. Further increase in the amount of potassium led to complete deactivation. Changes in the structural and chemical state of ceria and the degradation of surface acidity were the primary reasons for the deactivation. Ceria particles grew and amorphous ceria transformed into ceria crystals after adding potassium. As a result, the amount of ceria defects as well as oxygen vacancies was reduced which ultimately lowered the rate of ceria reduction and redox cycle. KCl and K_2SO_4 showed greater effect on the changes of ceria state than KNO_3. Potassium could destroy the acid sites, leading to the decline of ammonia adsorption capability. The introduction of Cl^- from KCl could be combined with Ce to form cerium chloride; hence Ce-centered Lewis acid sites were destroyed by Cl^-. The deposition of K_2SO_4 on catalyst surface will reduce the exposure of active sites for the SCR reaction. Cl and S have always coexisted with K biofuels and their concentrations are always high; thus the deactivation of Ce/TiO_2 utilized in biofuel boilers will be more significant than that in coal-fired boilers.

Conflict of Interests

The authors declare that there is no conflict of interests regarding the publication of this paper.

Acknowledgments

This research is financially supported by the National Natural Science Foundation of China (NSFC-51306068), the Project of the Science and Technology Program of Guangdong Province (2014A020216015), the Special Fund for Environ-scientific Research in the Public Interest (201509013), the Key Laboratory for Water and Air Pollution Control, Guangdong Province (no. 2011A060901002), and the Central-Level Non-profit Scientific Institutes for Basic R&D Operations.

References

[1] F. Liu, Y. Yu, and H. He, "Environmentally-benign catalysts for the selective catalytic reduction of NOx from diesel engines: structure-activity relationship and reaction mechanism aspects," *Chemical Communications*, vol. 50, no. 62, pp. 8445–8463, 2014.

[2] R. Q. Long and R. T. Yang, "Superior Fe-ZSM-5 catalyst for selective catalytic reduction of nitric oxide by ammonia," *Journal of the American Chemical Society*, vol. 121, no. 23, pp. 5595–5596, 1999.

[3] W. Xu, Y. Yu, C. Zhang, and H. He, "Selective catalytic reduction of NO by NH_3 over a Ce/TiO_2 catalyst," *Catalysis Communications*, vol. 9, no. 6, pp. 1453–1457, 2008.

[4] F. Liu, H. He, and C. Zhang, "Novel iron titanate catalyst for the selective catalytic reduction of NO with NH_3 in the medium temperature range," *Chemical Communications*, no. 17, pp. 2043–2045, 2008.

[5] Z. Lian, F. Liu, H. He, X. Shi, J. Mo, and Z. Wu, "Manganese-niobium mixed oxide catalyst for the selective catalytic reduction of NO_x with NH_3 at low temperatures," *Chemical Engineering Journal*, vol. 250, pp. 390–398, 2014.

[6] B. Dou, G. Lv, C. Wang, Q. Hao, and K. Hui, "Cerium doped copper/ZSM-5 catalysts used for the selective catalytic reduction of nitrogen oxide with ammonia," *Chemical Engineering Journal*, vol. 270, pp. 549–556, 2015.

[7] L. Qu, C. Li, G. Zeng et al., "Support modification for improving the performance of MnO_x-CeO_y/γ-Al_2O_3 in selective catalytic reduction of NO by NH_3," *Chemical Engineering Journal*, vol. 242, pp. 76–85, 2014.

[8] X. Chen, C. Cen, Z. Tang et al., "The key role of ph value in the synthesis of titanate nanotubes-loaded manganese oxides as a superior catalyst for the selective catalytic reduction of NO with NH_3," *Journal of Nanomaterials*, vol. 2013, Article ID 871528, 7 pages, 2013.

[9] Y. Liu, W. Yao, X. Cao et al., "Supercritical water syntheses of Ce_xTiO_2 nano-catalysts with a strong metal-support interaction for selective catalytic reduction of NO with NH_3," *Applied Catalysis B: Environmental*, vol. 160-161, no. 1, pp. 684–691, 2014.

[10] L. Chen, J. Li, M. Ge, and R. Zhu, "Enhanced activity of tungsten modified CeO_2/TiO_2 for selective catalytic reduction of NOx with ammonia," *Catalysis Today*, vol. 153, no. 3-4, pp. 77–83, 2010.

[11] Y. Zheng, A. D. Jensen, J. E. Johnsson, and J. R. Thøgersen, "Deactivation of V_2O_5-WO_3-TiO_2 SCR catalyst at biomass fired power plants: elucidation of mechanisms by lab- and pilot-scale experiments," *Applied Catalysis B: Environmental*, vol. 83, no. 3-4, pp. 186–194, 2008.

[12] D. Nicosia, I. Czekaj, and O. Kröcher, "Chemical deactivation of V_2O_5/WO_3-TiO_2 SCR catalysts by additives and impurities from fuels, lubrication oils and urea solution: part II. Characterization study of the effect of alkali and alkaline earth metals," *Applied Catalysis B: Environmental*, vol. 77, no. 3-4, pp. 228–236, 2008.

[13] P. Kern, M. Klimczak, T. Heinzelmann, M. Lucas, and P. Claus, "High-throughput study of the effects of inorganic additives and poisons on NH_3-SCR catalysts. Part II: fe–zeolite catalysts," *Applied Catalysis B: Environmental*, vol. 95, no. 1-2, pp. 48–56, 2010.

[14] A. L. Kustov, S. B. Rasmussen, R. Fehrmann, and P. Simonsen, "Activity and deactivation of sulphated TiO_2- and ZrO_2-based V, Cu, and Fe oxide catalysts for NO abatement in alkali containing flue gases," *Applied Catalysis B: Environmental*, vol. 76, no. 1-2, pp. 9–14, 2007.

[15] H. Wang, X. Chen, S. Gao, Z. Wu, Y. Liu, and X. Weng, "Deactivation mechanism of Ce/TiO_2 selective catalytic reduction catalysts by the loading of sodium and calcium salts," *Catalysis Science & Technology*, vol. 3, no. 3, pp. 715–722, 2013.

[16] J. Ma, Z. Si, D. Weng, X. Wu, and Y. Ma, "Potassium poisoning on Cu-SAPO-34 catalyst for selective catalytic reduction of NO_x with ammonia," *Chemical Engineering Journal*, vol. 267, pp. 191–200, 2015.

[17] Y. Peng, J. Li, W. Si et al., "Ceria promotion on the potassium resistance of $MnOx/TiO_2$ SCR catalysts: an experimental and DFT study," *Chemical Engineering Journal*, vol. 269, pp. 44–50, 2015.

[18] Å. Kling, C. Andersson, Å. Myringer, D. Eskilsson, and S. G. Järås, "Alkali deactivation of high-dust SCR catalysts used for NO_x reduction exposed to flue gas from 100 MW-scale biofuel and peat fired boilers: influence of flue gas composition," *Applied Catalysis B: Environmental*, vol. 69, no. 3-4, pp. 240–251, 2007.

[19] Y. P. Li, T. J. Wang, C. Z. Wu et al., "Effect of alkali vapor exposure on Ni-MgO/γ-Al_2O_3/cordierite monolithic catalyst for biomass fuel gas reforming," *Industrial & Engineering Chemistry Research*, vol. 49, no. 7, pp. 3176–3183, 2010.

[20] F. Tang, B. Xu, H. Shi, J. Qiu, and Y. Fan, "The poisoning effect of Na^+ and $Ca2^+$ ions doped on the V_2O_5/TiO_2 catalysts for selective catalytic reduction of NO by NH_3," *Applied Catalysis B: Environmental*, vol. 94, no. 1-2, pp. 71–76, 2010.

[21] F. Larachi, J. Pierre, A. Adnot, and A. Bernis, "Ce 3d XPS study of composite $Ce_xMn_{1-x}O_{2-y}$ wet oxidation catalysts," *Applied Surface Science*, vol. 195, no. 1–4, pp. 236–250, 2002.

[22] E. Beche, P. Charvin, D. Perarnau, S. Abanades, and G. Flamant, "Ce 3d XPS investigation of cerium oxides and mixed cerium oxide ($Ce_xTi_yO_z$)," *Surface and Interface Analysis*, vol. 40, no. 3-4, pp. 264–267, 2008.

[23] S. Yang, Y. Feng, J. Wan, W. Zhu, and Z. Jiang, "Effect of CeO_2 addition on the structure and activity of $RuO2/\gamma$-Al_2O_3 catalyst," *Applied Surface Science*, vol. 246, no. 1–3, pp. 222–228, 2005.

[24] S. Yang, W. Zhu, Z. Jiang, Z. Chen, and J. Wang, "The surface properties and the activities in catalytic wet air oxidation over CeO_2-TiO_2 catalysts," *Applied Surface Science*, vol. 252, no. 24, pp. 8499–8505, 2006.

[25] S. Gao, X. Chen, H. Wang et al., "Ceria supported on sulfated zirconia as a superacid catalyst for selective catalytic reduction of NO with NH_3," *Journal of Colloid and Interface Science*, vol. 394, pp. 515–521, 2013.

[26] G. Busca, L. Lietti, G. Ramis, and F. Berti, "Chemical and mechanistic aspects of the selective catalytic reduction of NO_x by ammonia over oxide catalysts: a review," *Applied Catalysis B: Environmental*, vol. 18, no. 1-2, pp. 1–36, 1998.

[27] J. Li, H. Chang, L. Ma, J. Hao, and R. T. Yang, "Low-temperature selective catalytic reduction of NO_x with NH_3 over metal oxide and zeolite catalysts—a review," *Catalysis Today*, vol. 175, no. 1, pp. 147–156, 2011.

[28] L. Xue, C. Zhang, H. He, and Y. Teraoka, "Catalytic decomposition of N_2O over CeO_2 promoted Co_3O_4 spinel catalyst," *Applied Catalysis B: Environmental*, vol. 75, no. 3-4, pp. 167–174, 2007.

[29] S. Damyanova, C. A. Perez, M. Schmal, and J. M. C. Bueno, "Characterization of ceria-coated alumina carrier," *Applied Catalysis A: General*, vol. 234, no. 1-2, pp. 271–282, 2002.

[30] X. Liu, K. Zhou, L. Wang, B. Wang, and Y. Li, "Oxygen vacancy clusters promoting reducibility and activity of ceria nanorods," *Journal of the American Chemical Society*, vol. 131, no. 9, pp. 3140–3141, 2009.

[31] C. T. Campbell and C. H. F. Peden, "Oxygen vacancies and catalysis on ceria surfaces," *Science*, vol. 309, no. 5735, pp. 713–714, 2005.

[32] F. Esch, S. Fabris, L. Zhou et al., "Electron localization determines defect formation on ceria substrates," *Science*, vol. 309, no. 5735, pp. 752–755, 2005.

[33] P. Dutta, S. Pal, M. S. Seehra, Y. Shi, E. M. Eyring, and R. D. Ernst, "Concentration of Ce^{3+} and oxygen vacancies in cerium oxide nanoparticles," *Chemistry of Materials*, vol. 18, no. 21, pp. 5144–5146, 2006.

[34] L. Lisi, G. Lasorella, S. Malloggi, and G. Russo, "Single and combined deactivating effect of alkali metals and HCl on commercial SCR catalysts," *Applied Catalysis B: Environmental*, vol. 50, no. 4, pp. 251–258, 2004.

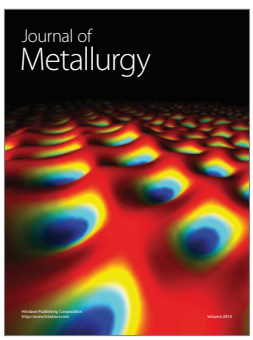

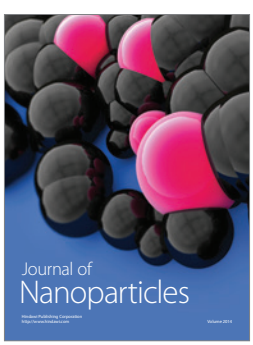

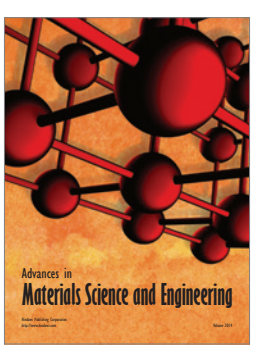

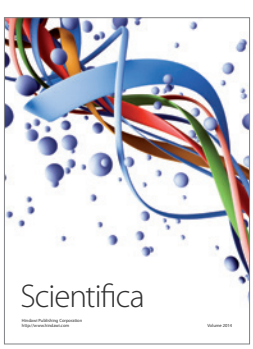

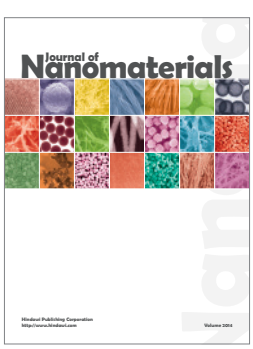

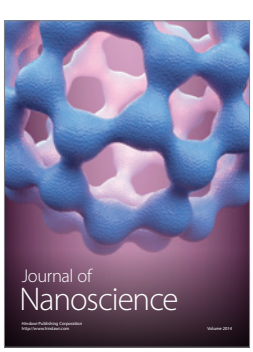

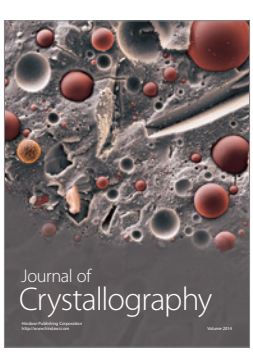

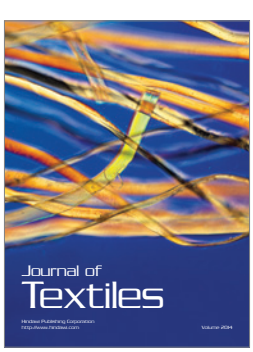

Hindawi

Submit your manuscripts at
http://www.hindawi.com